International Journal of Machine Tools & Manufacture 49 (2009) 25–35

Contents lists available at ScienceDirect

International Journal of Machine Tools & Manufacture

journal homepage: www.elsevier.com/locate/ijmactool

A closed-form approach for identification of dynamical contact parameters in spindle–holder–tool assemblies

O. Özşahin [a], A. Ertürk [a,1], H.N. Özgüven [a], E. Budak [b,*]

[a] Department of Mechanical Engineering, Middle East Technical University, 06531 Ankara, Turkey
[b] Faculty of Engineering and Natural Sciences, Sabanci University, Orhanli, Tuzla, 34956 Istanbul, Turkey

ARTICLE INFO

Article history:
Received 16 May 2008
Received in revised form
17 August 2008
Accepted 24 August 2008
Available online 17 September 2008

Keywords:
Chatter stability
Machine tool dynamics
Contact dynamics
Parameter identification

ABSTRACT

Accurate identification of contact dynamics is very crucial in predicting the dynamic behavior and chatter stability of spindle–tool assemblies in machining centers. It is well known that the stability lobe diagrams used for predicting regenerative chatter vibrations can be obtained from the tool point frequency response function (FRF) of the system. As previously shown by the authors, contact dynamics at the spindle–holder and holder–tool interfaces as well as the dynamics of bearings affect the tool point FRF considerably. Contact stiffness and damping values alter the frequencies and peak values of dominant vibration modes, respectively. Fast and accurate identification of contact dynamics in spindle–tool assemblies has become an important issue in the recent years. In this paper, a new method for identifying contact dynamics in spindle–holder–tool assemblies from experimental measurements is presented. The elastic receptance coupling equations are employed in a simple manner and closed-form expressions are obtained for the stiffness and damping parameters of the joint of interest. Although this study focuses on the contact dynamics at the spindle–holder and holder–tool interfaces of the assembly, the identification approach proposed in this paper might as well be used for identifying the dynamical parameters of bearings, spindle–holder interface and as well as other critical joints. After presenting the mathematical theory, an analytical case study is given for demonstration of the identification approach. Experimental verification is provided for identification of the dynamical contact parameters at the holder–tool interface of a spindle–holder–tool assembly.

1. Introduction

Self-excited vibration of machine tools during the cutting process (the so-called *regenerative chatter*) is caused by the cutting tool–work piece dynamic interaction and results in process instability, poor surface finish and reduced material removal rate. Modeling of chatter mechanism for minimizing its catastrophic consequences has been studied in detail for the last 50 years [1–5]. It is well known that the regeneration effect is due to the phase between two vibration waves during the subsequent cuts on a surface [6], and this phase is minimized for certain cutting speeds. Stability lobe diagrams provide stable depth of cut–spindle speed combinations and they have been used for predicting chatter stability for decades. The literature includes both numerical [3] and analytical [4,5] approaches for generating stability lobe diagrams of spindle–tool assemblies. Regardless of the approach used, a common point of the models used for generation of stability lobe diagrams is the requirement of the tool point frequency response function (FRF) of the assembly. Although experimental modal analysis by simple impact testing is the typical technique employed for obtaining the tool point FRF [6], recently, researchers have attempted to obtain the tool point FRF semi-analytically to minimize experimentation and save time in practical applications. Schmitz et al. [7–9] implemented the well-known receptance coupling theory of structural dynamics [10–12] in order to couple the experimentally obtained dynamics of spindle–holder assembly and the analytically obtained tool dynamics by using the contact dynamics at the holder–tool interface. The aim was to make only one experiment at the holder tip and then to obtain the tool point FRF of the assembly for different tool overhang lengths through the receptance coupling equations [7–9]. Provided that the dynamical contact parameters at the holder–tool interface are known accurately, this semi-analytical approach can provide accurate results and save considerable time.

Several improvements were made to the approach proposed by Schmitz et al. [7–9] in the last 5 years. Park et al. [13] included the

* Corresponding author. Tel.: +90 216 483 9519; fax: +90 216 483 9550.
E-mail address: ebudak@sabanciuniv.edu (E. Budak).
[1] Presently at the Department of Engineering Science and Mechanics, Virginia Polytechnic Institute and State University, Blacksburg, VA 24061, USA.

0890-6955/$ - see front matter © 2008 Elsevier Ltd. All rights reserved.
doi:10.1016/j.ijmachtools.2008.08.007

rotational degree-of-freedom at the tool holder–tool joint. Kivanc and Budak [14] modeled the tool as a two-segment beam considering the changing area moment of inertia for more accurate results. They [14] also studied the effects of the contact length and the clamping torque on the holder–tool contact stiffness and damping properties. Duncan and Schmitz [15] improved the use of receptance coupling approach to handle different holder types by extending it to the coupling of holder segments. It should be underlined again that the accuracy of these models strongly depends on the accurate identification of dynamical contact parameters at the holder–tool interface. Accurate modeling and identification of contact mechanics has been an important problem in several engineering applications, and its nature has been investigated by scientists and engineers for decades [16]. Expectedly, it has also been subject to research in machine tool engineering where some researchers investigated the spindle–holder interface dynamics for analyzing and improving structural stability [17–21]. Recently, Schmitz et al. [22] introduced off-diagonal elements to the diagonal joint stiffness matrix used in their early work [7–9] to account for the translations imposed by moments and rotations caused by forces. More recently, Ahmadi and Ahmadian [23] considered the holder–tool interface as a distributed elastic layer to model the change in the normal contact pressure along the joint interface.

Ertürk et al. [24] proposed an experimentally verified [25,26] analytical model for predicting the tool point FRF by combining the receptance coupling and structural modification techniques where all components of the spindle–holder–tool assembly were modeled analytically with the Timoshenko beam theory. They [24] formed the individual system components (spindle, holder and tool) by *rigid receptance coupling* of free–free Timoshenko beams and included the dynamics of bearings to the spindle by structural modification with an efficient dynamic coupling algorithm. Then, these three main components of the system were combined by *elastic receptance coupling* with the information of contact dynamics at the spindle–holder and holder–tool. The analytical model proposed for the prediction of tool point FRF [24] was shown to be very efficient in predicting chatter stability [26] when it is combined with the analytical stability lobe diagram model presented by Budak and Altintas [4,5]. The influence of bearing and interface dynamics on the tool point FRF was also studied [27] by using the analytical model proposed. It was observed that the variations in the dynamical contact parameters at the spindle–holder and holder–tool interfaces as well as bearing dynamics have a strong effect on the resulting tool point FRF of the system. For a typical system, it was identified that the dynamical contact parameters (stiffness and damping) at the spindle–holder and holder–tool interfaces affect the dominant elastic modes of the tool point FRF [27]. Variations of the translational contact stiffness were found to be affecting the frequencies of the elastic modes, whereas the variations in the translational contact damping altered the peak values of these respective modes. Furthermore, for a typical assembly, an uncoupled trend was observed between the effects of the contact dynamics at the spindle–holder and holder–tool interfaces such that the dynamics of the former interface controlled the spindle bending mode of the assembly, whereas that of the latter interface controlled the tool mode of the assembly (which were the first and the second elastic modes of the assembly used by Ertürk et al. [27], respectively). From this observation, the important suggestion made was identifying the dynamical contact parameters of an interface from the respective vibration mode(s) they control. Considering the fact that the earlier work [7–9] used the nonlinear least square error minimization for identifying the contact parameters, the approach suggested by Ertürk et al. [27] was very practical to implement and time saving for two reasons. First, there is no need to use the entire frequency band of the experimental FRF, since a simple effect analysis made by perturbation of the contact parameters in the model yields the frequency range(s) where one should identify those parameters. Indeed, theoretically, it is meaningless to identify a damping parameter by minimizing the error in the analytical (or semi-analytical) FRF at the structural stiffness/mass controlled *off-resonance* frequencies. Secondly, due to the nonlinearity of the least square error minimization approach, it is not uncommon to obtain more than one solution set of the contact parameters since the numerical solution may converge to the results for a local minimum. The approach suggested [27] avoids both of these problems and reduces the time required for identifying the dynamical contact parameters not only at the holder–tool interface but also at the spindle–holder interface as well as the dynamical parameters of bearings.

In this paper, a new approach for identification of dynamical contact parameters in spindle–holder–tool assemblies is presented. The elastic receptance coupling equations [24] used for coupling the system components are rearranged to give the complex stiffness matrix of the joint (interface) of interest (e.g., spindle–holder or holder–tool joint). After expressing the fully populated complex stiffness matrix at the joint of interest in terms of the analytical and experimental receptance matrices, the contact stiffness and damping parameters are extracted by utilizing the conclusions of our previous work [27] summarized in the previous paragraph. The identification approach suggested is first used in a case study for analytical demonstration. Then, it is verified experimentally for a spindle–holder–tool assembly with a focus on the holder–tool interface. Although the approach presented in this paper concentrates on the contact dynamics at the spindle–holder and holder–tool interfaces, it can also be used to identify the bearing dynamics and the dynamics of the other critical joints of a machine tool assembly.

2. Theory

2.1. Mathematical background

A typical spindle–holder–tool assembly and its components are shown in Fig. 1. In the analytical model proposed by Ertürk et al. [24],

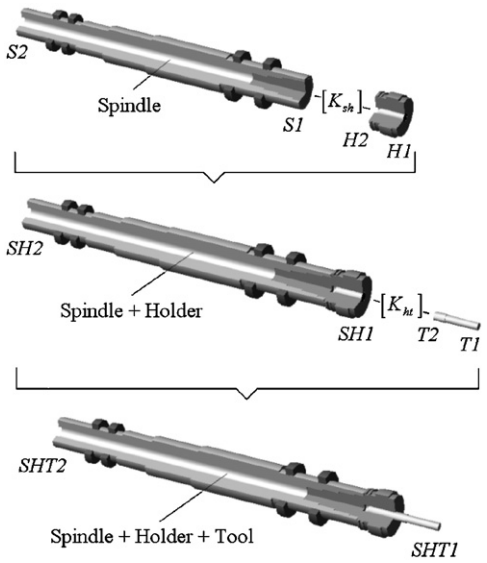

Fig. 1. Components of spindle–holder–tool assembly and the complex stiffness matrices of spindle–holder and holder–tool interfaces.

the individual receptance matrices of the assembly are obtained by rigid receptance coupling of free–free Timoshenko beams and the bearing dynamics is added to the spindle by structural modification. After obtaining the end-point receptance matrices of spindle (S), holder (H) and tool (T), they are assembled through the complex stiffness matrices of the spindle–holder and holder–tool interfaces, which are denoted in Fig. 1 by $[K_{sh}]$ and $[K_{ht}]$, respectively. This way, the point receptance matrix of the entire assembly at the tool tip is obtained. For instance, the following equations represent the elastic coupling of the spindle and the holder FRFs to obtain the end-point receptances of the spindle–holder subassembly:

$$[SH_{11}] = [H_{11}] - [H_{12}][[H_{22}] + [K_{sh}]^{-1} + [S_{11}]]^{-1}[H_{21}] \quad (1)$$

$$[SH_{12}] = [H_{12}][[H_{22}] + [K_{sh}]^{-1} + [S_{11}]]^{-1}[S_{12}] \quad (2)$$

$$[SH_{21}] = [S_{21}][[H_{22}] + [K_{sh}]^{-1} + [S_{11}]]^{-1}[H_{21}] \quad (3)$$

$$[SH_{22}] = [S_{22}] - [S_{21}][[H_{22}] + [K_{sh}]^{-1} + [S_{11}]]^{-1}[S_{12}] \quad (4)$$

Then, the point receptance matrix of the assembly at the tool tip is obtained from

$$[SHT_{11}] = [T_{11}] - [T_{12}][[T_{22}] + [K_{ht}]^{-1} + [SH_{11}]]^{-1}[T_{21}] \quad (5)$$

whose first element is the so-called *tool point FRF*, which is required for generating the stability lobe diagrams.

The elements of these matrices and their derivations by modal analysis can be found in the relevant work [24,28]. In the following, these elastic receptance coupling equations are rearranged for obtaining closed-form expressions to predict the complex stiffness matrices of holder–tool and spindle–holder interfaces. Thus the dynamical contact parameters, i.e. stiffness and damping parameters, of these interfaces can be extracted in closed form.

2.2. Identification of contact dynamics at the holder–tool interface

The end-point receptance matrix of the assembly given by Eq. (5) can be rearranged to give Eq. (6) for the complex stiffness matrix of the holder–tool interface:

$$[K_{ht}] = [[[T_{12}]^{-1}[[T_{11}] - [SHT_{11}]][T_{21}]^{-1}]^{-1} - [T_{22}] - [SH_{11}]]^{-1} \quad (6)$$

Here, the complex stiffness matrix given by Eq. (6) was defined in the elastic receptance coupling equations [24] as

$$[K_{ht}] = \begin{bmatrix} k_y^{ht} + i\omega c_y^{ht} & 0 \\ 0 & k_\theta^{ht} + i\omega c_\theta^{ht} \end{bmatrix} \quad (7)$$

where no coupling exists between the linear displacements and moments as well as between the angular displacements and forces at the interface (since the off-diagonal elements are zero). Schmitz et al. [23] replaced this classical form of the joint stiffness matrix with the following fully populated matrix to account for the linear displacements imposed by moments and angular displacements caused by forces (and this is what is considered in the remaining part of this paper):

$$[K_{ht}] = \begin{bmatrix} k_{yf}^{ht} + i\omega c_{yf}^{ht} & k_{ym}^{ht} + i\omega c_{ym}^{ht} \\ k_{\theta f}^{ht} + i\omega c_{\theta f}^{ht} & k_{\theta m}^{ht} + i\omega c_{\theta m}^{ht} \end{bmatrix} \quad (8)$$

where k_{yf}^{ht} is the linear displacement-to-force stiffness, c_{yf}^{ht} is the linear displacement-to-force damping, k_{ym}^{ht} is the linear displacement-to-moment stiffness, c_{ym}^{ht} is the linear displacement-to-moment damping, $k_{\theta f}^{ht}$ is the angular displacement-to-force stiffness, $c_{\theta f}^{ht}$ is the angular displacement-to-force damping, $k_{\theta m}^{ht}$ is the angular displacement-to-moment stiffness and $c_{\theta m}^{ht}$ is the angular displacement-to-moment damping of the holder–tool interface, ω is the excitation frequency and i is the unit imaginary number. Hence, the fully populated form of the complex stiffness matrix of the holder–tool interface includes the dynamics information of the linear displacement-to-moment and angular displacement-to-force coupling at the interface. Although the off-diagonal stiffness and damping terms in Eq. (8) are represented by different terms to handle experimental inaccuracies, one should expect $k_{ym}^{ht} \cong k_{\theta f}^{ht}$ and $c_{ym}^{ht} \cong c_{\theta f}^{ht}$ so that the linear receptance coupling formulation is in agreement with the Betti–Maxwell reciprocity theorem of linear elasticity [29]. The joint stiffness matrix, in agreement with this theorem, is defined to be symmetric in the relevant literature of structural coupling with elastic joints (see, for instance, Liu and Ewins [12]). Otherwise, the *forward receptance coupling* formulation given by Eq. (5) may yield an asymmetric tool point receptance matrix even for symmetric subsystem matrices, violating the aforementioned theorem. Thus, theoretically, Eq. (8) has six independent elements that represent the dynamical contact information of the holder–tool joint. However, considering the possibility of experimental inaccuracies, it is reasonable to define eight parameters. Once the identification process is complete, one can check if $k_{ym}^{ht} \cong k_{\theta f}^{ht}$ and $c_{ym}^{ht} \cong c_{\theta f}^{ht}$ are satisfied. A possible disagreement of these off-diagonal parameters might be due to experimental inaccuracies (e.g., due to finite-difference approximation of the linear displacement-to-moment and angular displacement-to-force FRFs) or it might as well be due to the failure of linear contact dynamics assumption.

It is clear from Eq. (6) that the receptance matrices of the cutting tool (with free–free boundary conditions), and the tip-point receptance matrix of the spindle–holder subassembly (without the part of the cutting tool outside the holder) as well as the tip-point receptance matrix of the complete assembly are required for obtaining the complex stiffness matrix of holder–tool interface. The receptance matrices of the cutting tool in free–free boundary conditions, which are denoted by $[T_{11}]$, $[T_{12}]$, $[T_{21}]$ and $[T_{22}]$, can be obtained analytically as follows [24]:

$$[T_{11}] = \begin{bmatrix} H_{11}^t & L_{11}^t \\ N_{11}^t & P_{11}^t \end{bmatrix}, \quad [T_{12}] = \begin{bmatrix} H_{12}^t & L_{12}^t \\ N_{12}^t & P_{12}^t \end{bmatrix}$$
$$[T_{21}] = \begin{bmatrix} H_{21}^t & L_{21}^t \\ N_{21}^t & P_{21}^t \end{bmatrix}, \quad [T_{22}] = \begin{bmatrix} H_{22}^t & L_{22}^t \\ N_{22}^t & P_{22}^t \end{bmatrix} \quad (9)$$

where the receptance functions in the above matrices are defined by the following equations and superscript t stands for the tool:

$$H_{mn} = \frac{w_m}{f_n}, \quad N_{mn} = \frac{\theta_m}{f_n}, \quad L_{mn} = \frac{w_m}{m_n}, \quad P_{mn} = \frac{\theta_m}{m_n} \quad (10)$$

In Eq. (9), w is the transverse displacement, θ is the bending slope, f is the transverse force, m is the bending moment and the subscripts stand for the points of interest over the length of the tool. For instance, if the tool is to be modeled as a uniform beam, the elements of its point receptance matrix $[T_{11}]$ are[2]

$$H_{11}^t = \frac{-1}{\rho A L \omega^2} + \frac{-3}{\rho A L \omega^2} + \sum_{r=1}^{\infty} \frac{\phi_r(L)\phi_r(L)}{(1+i\gamma)\omega_r^2 - \omega^2} \quad (11)$$

$$N_{11}^t = \frac{-6}{\rho A L^2 \omega^2} + \sum_{r=1}^{\infty} \frac{\phi_r'(L)\phi_r(L)}{(1+i\gamma)\omega_r^2 - \omega^2} \quad (12)$$

[2] If the tool is to be modeled as a two-segment beam, it is a straightforward practice to couple the analytical equations of two free–free beams of different diameters and lengths [24].

$$L_{11}^{t} = \frac{-6}{\rho A L^2 \omega^2} + \sum_{r=1}^{\infty} \frac{\phi_r(L)\phi_r'(L)}{(1+i\gamma)\omega_r^2 - \omega^2} \tag{13}$$

$$P_{11}^{t} = \frac{-12}{\rho A L^3 \omega^2} + \sum_{r=1}^{\infty} \frac{\phi_r'(L)\phi_r'(L)}{(1+i\gamma)\omega_r^2 - \omega^2} \tag{14}$$

where ρ is the density, A is the cross-sectional area, L is the length and γ is the loss factor of the tool. Furthermore, ω_r is the rth natural frequency, $\phi_r(x)$ is the rth mode shape for transverse displacement of the tool and $\phi_r'(x)$ is the derivative of $\phi_r(x)$ with respect to the axial independent displacement variable x. It should be clarified at this point that, since there is no shear deformation at the end points of the *free–free* cutting tool (i.e., at $x = 0$ and L), the bending slope at these points are identical to the total slope [28]. Thus, for simplicity, $\phi_r'(L)$ is used in the receptance functions given here as well as in Ref. [23] rather than using $\psi_r(L)$, where $\psi_r(x)$ is the exact bending slope eigenfunction [28].

The tool point receptance matrix $[SHT_{11}]$ of the spindle–holder–tool assembly required in Eq. (6) should be obtained experimentally. The first element H_{11}^{sht} of this matrix can be obtained simply by performing an impact test at the tool tip of the assembly. Although obtaining the remaining receptances L_{11}^{sht}, N_{11}^{sht} and P_{11}^{sht} is not simple, one can employ a first-order or a second-order finite-difference solution for approximating these FRFs [30]. In the proposed method by Duarte and Ewins [30], if the first-order approximation is used, measurements are taken from two locations; however in the second-order approximation measurements are taken from three distinct locations. Most crucial part of the approximation method is that the accuracy of the method is highly dependent on the order of the approximation and spacing between measurement points. As expressed by Duarte and Ewins [30], higher-order approximation requires smaller spacing between measurement points for the angular displacement-to-force FRFs and requires larger spacing for the angular displacement-to-moment FRFs. Therefore, for the four receptance matrices that define matrix $[SHT_{11}]$, one should carefully perform the experimental measurements on the cutting tool of the assembly so that H_{11}^{sht}, L_{11}^{sht}, N_{11}^{sht} and P_{11}^{sht} are obtained by a suitable approximation method and $[SHT_{11}]$ can be constructed. It is also required to obtain the receptance matrix $[SH_{11}]$ of the spindle–holder subassembly (without the cutting tool outside the holder) experimentally. The procedure of obtaining the elements of this matrix is similar to that used for generating $[SHT_{11}]$.

Having obtained all the receptance matrices at the right-hand side of Eq. (6) analytically and experimentally, one can obtain the complex stiffness matrix of the holder–tool joint, elements of which give the stiffness and damping parameters of the holder–tool interface: k_{yf}^{ht}, c_{yf}^{ht}, k_{ym}^{ht}, c_{ym}^{ht}, $k_{\theta f}^{ht}$, $c_{\theta f}^{ht}$, $k_{\theta m}^{ht}$, $k_{\theta m}^{ht}$.

2.3. Identification of contact dynamics at the spindle–holder interface

A similar approach can be used for identifying the spindle–holder interface dynamics; however, now there are two ways of approaching to the problem. One can consider the interface either for the spindle–holder (SH) subassembly (without the tool outside the holder) or for the spindle–holder–tool (SHT) assembly (where the interface is defined between the spindle (S) and the holder–tool (HT) subassemblies).

For the first case where the cutting tool is not connected to the assembly, Eq. (1) applies for the elastic coupling of spindle and holder and it can be rearranged to give the complex stiffness matrix of spindle–holder interface as

$$[K_{sh}] = [[[H_{12}]^{-1}[[H_{11}] - [SH_{11}]][H_{21}]^{-1}]^{-1} - [H_{22}] - [S_{11}]]^{-1} \tag{15}$$

where

$$[K_{sh}] = \begin{bmatrix} k_{yf}^{sh} + i\omega c_{yf}^{sh} & k_{ym}^{sh} + i\omega c_{ym}^{sh} \\ k_{\theta f}^{sh} + i\omega c_{\theta f}^{sh} & k_{\theta m}^{sh} + i\omega c_{\theta m}^{sh} \end{bmatrix} \tag{16}$$

is the fully populated complex stiffness matrix of the spindle–holder interface. The elements in Eq. (16) are analogous to those of the complex stiffness matrix of the holder–tool interface given by Eq. (8). Furthermore, the discussion regarding the off-diagonal elements in Eq. (8) is also valid for the off-diagonal elements in Eq. (16).

Alternatively, one can consider the coupling between the spindle (S) and holder–tool (HT) subassemblies for which the following elastic receptance coupling equation can be written as

$$[SHT_{11}] = [HT_{11}] - [HT_{12}][[HT_{22}] + [K_{sh}]^{-1} + [S_{11}]]^{-1}[HT_{21}] \tag{17}$$

and it can be rearranged to yield

$$[K_{sh}] = [[[HT_{12}]^{-1}[[HT_{11}] - [SHT_{11}]][HT_{21}]^{-1}]^{-1} - [HT_{22}] - [S11]]^{-1} \tag{18}$$

which is as defined by Eq. (16).

Among these two approaches of obtaining the interface dynamics at the spindle–holder interface, the former one given by Eq. (15) can be preferable where the cutting tool is not connected. This allows obtaining the receptance matrices $[H_{11}]$, $[H_{12}]$, $[H_{21}]$ and $[H_{22}]$ of the *free–free* holder analytically as the free–free receptances $[T_{11}]$, $[T_{12}]$, $[T_{21}]$ and $[T_{22}]$ of the cutting tool were obtained in the previous section. Then, the end-point receptance matrices $[SHT_{11}]$ and $[S_{11}]$ should be obtained by using the finite-difference approximation, which was employed for obtaining $[SHT_{11}]$ and $[SH_{11}]$ in the previous section. In the second approach for obtaining $[K_{sh}]$ suggested by Eq. (17), it is required to obtain the end-point receptance matrices of holder–tool (HT) subassembly, which might be a more involved problem since this subassembly already has an interface to be identified by the approach suggested in the previous section. Nevertheless, after obtaining $[K_{ht}]$ by following the procedure given in the previous section, one can couple the dynamics of the holder (H) and tool (T) to obtain the end-point receptances of the holder–tool (HT) subassembly and use in Eq. (17) along with the finite-difference approximations of $[SHT_{11}]$ and $[S_{11}]$ to obtain $[K_{sh}]$.

3. Analytical case study

In this section, an analytical case study for the identification approach described is provided. For convenience and in order to check the agreement of the resulting trends with our previous work on interface dynamics [27], the assembly that was used in references [24,27] is used here for the analytical case study (with different contact parameters). The dynamical contact parameters of the assembly at the holder–tool interface are given in Table 1. In order to maintain the symmetry based on the discussion given in

Table 1
Dynamical contact parameters at the holder–tool interface in the analytical case study

Linear displacement-to-force stiffness (N/m)	4.19×10^7
Linear displacement-to-force damping (N s/m)	54
Linear displacement-to-moment stiffness (N m/m)	2.06×10^6
Linear displacement-to-moment damping (N m s/m)	22.2
Angular displacement-to-force stiffness (N/rad)	2.06×10^6
Angular displacement-to-force damping (N s/rad)	22.2
Angular displacement-to-moment stiffness (N m/rad)	6.5×10^4
Angular displacement-to-moment damping (N m s/rad)	1

Section 2.2, the off-diagonal terms of the complex stiffness matrix are taken to be equal.

The tool point FRF of the assembly is obtained by using the analytical model [24] as shown in Fig. 2a, and this is the first element of the assembly matrix $[SHT_{11}]$ as mentioned previously. The analytical model also allows obtaining the tip-point receptance of the spindle–holder subassembly (without the tool outside the holder) as depicted in Fig. 2b, which is the first element of $[SH_{11}]$. The remaining 22 FRFs required for constructing the right-hand side of Eq. (6) can be obtained analytically in the same manner and the complex stiffness matrix $[K_{ht}]$ can be obtained. Then, the linear displacement-to-force, linear displacement-to-moment, angular displacement-to-force and angular displacement-to-moment complex stiffness functions of the holder–tool interface are the elements of $[K_{ht}]$, which are $k_{yf}^{ht}+i\omega c_{yf}^{ht}$, $k_{ym}^{ht}+i\omega c_{ym}^{ht}$, $k_{\theta f}^{ht}+i\omega c_{\theta f}^{ht}$ and $k_{\theta m}^{ht}+i\omega c_{\theta m}^{ht}$, respectively. Consequently, the real parts of these expressions directly give the stiffnesses, whereas the imaginary parts give the damping coefficients when they are divided by the frequency. As can be seen from Fig. 3a and b, the dynamical contact parameters of the holder–tool interface are, expectedly, exactly the same as the values entered as inputs to the analytical model (Table 1). It should be noted that the stiffness and damping parameters identified in Fig. 3 do not change with frequency. This is an expected result since the assumed frequency-independent (i.e., constant) contact parameters given in Table 1 were used to obtain the tool point FRF from Eq. (5). Thus, the same contact parameters are identified through Eq. (6) by using the receptance matrices of the assembly, cutting tool and the spindle–holder subassembly in the backward sense. If one assumed frequency-dependent forms for the contact parameters in the forward coupling equation, the resulting contact parameters identified from Eq. (6) would come out to be frequency dependent.

Now, the analytical coherence between the elements of the tip-point receptance matrix $[SHT_{11}]$ of the spindle–holder–tool assembly and the elements of the spindle–holder subassembly receptance matrix $[SH_{11}]$ will be distorted for simulating a more realistic scenario. Random number arrays with mean values of unity and standard deviations of 5% are generated in MATLAB® and they are multiplied with the FRFs of matrices $[SH_{11}]$ and $[SHT_{11}]$. In this way, the analytical coherence between the elements of these matrices is distorted. The first two elements of these distorted receptance matrices are displayed in Fig. 4a and b, respectively. Note that the identification theory implies obtaining the end-point FRFs of the free–free cutting tool analytically so the analytical FRFs of matrices $[T_{11}]$, $[T_{12}]$, $[T_{21}]$ and $[T_{22}]$ are untouched. Then, the stiffness and damping parameters of holder–tool interface are obtained and linear displacement-to-force stiffness and linear displacement-to-force damping are plotted against frequency in Fig. 5a and b. For the remaining contact parameters, similar deficiencies are observed as in Fig. 5a and b. Comparing the fully analytical case and distorted case, it is interesting to observe the deficiency and the noise generated in the predictions due to the distorted coherence of the analytical FRFs used in the identification equation. However, the results in Fig. 5a and b are promising and they are in perfect agreement with the results of the effect analysis performed and the parameter identification approach proposed in Ref. [27].

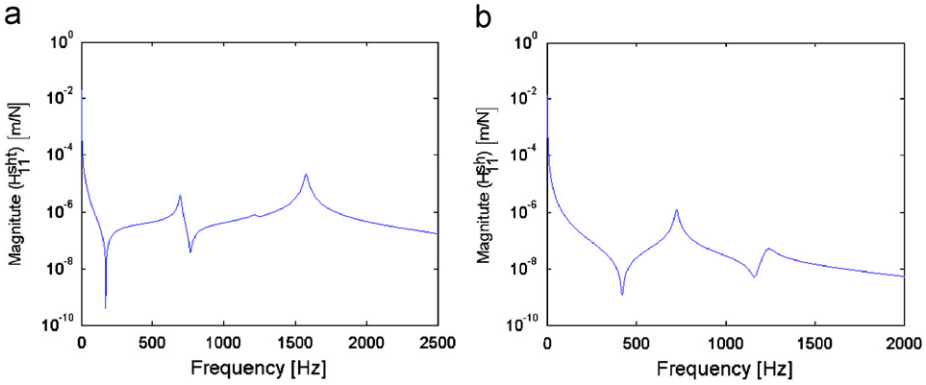

Fig. 2. (a) Analytically obtained tool point FRF (H_{11}^{sht}) of the spindle–holder–tool assembly and (b) the analytically obtained tip-point FRF (H_{11}^{sh}) of the spindle–holder subassembly.

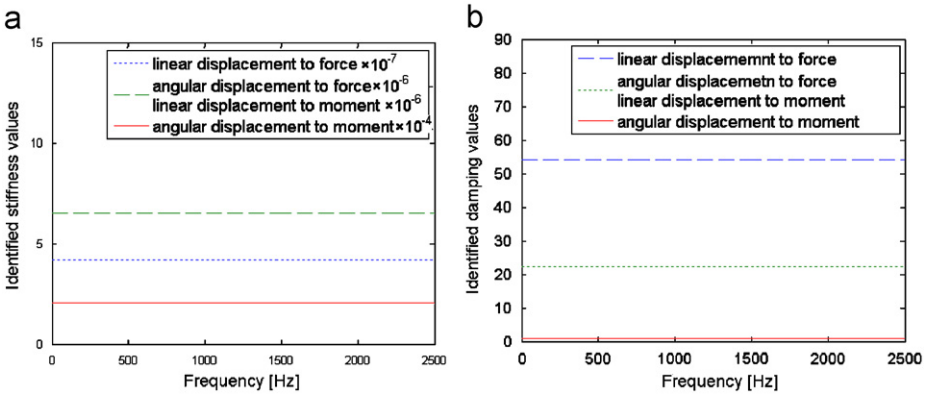

Fig. 3. Dynamical parameters at the holder–tool interface obtained from Eq. (6) by using the analytically obtained FRFs; (a) identified stiffness values and (b) identified damping values.

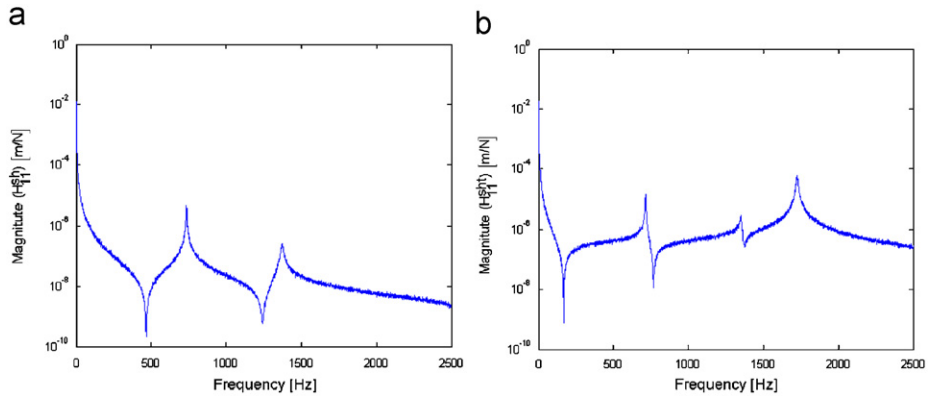

Fig. 4. (a) Distorted tip-point FRF (H_{11}^{sh}) of the spindle–holder subassembly and (b) distorted tool point FRF (H_{11}^{sht}) of the spindle–holder–tool assembly.

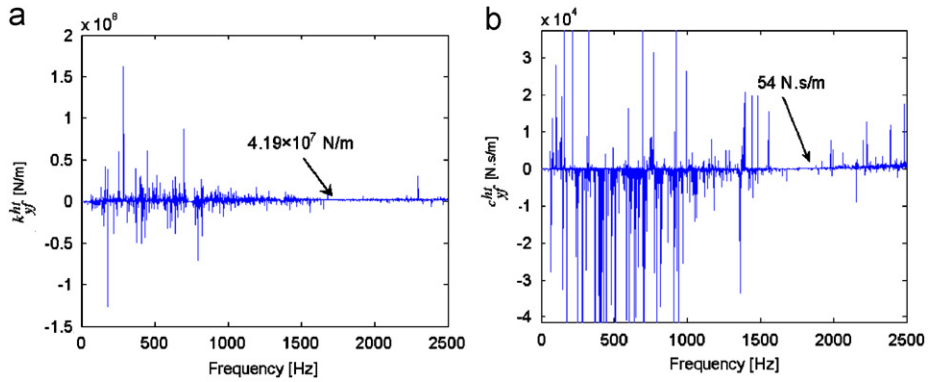

Fig. 5. Dynamical parameters at the holder–tool interface obtained from Eq. (6) by using the distorted FRFs; (a) linear displacement-to-force stiffness k_{yf}^{ht} and (b) linear displacement-to-force damping c_{yf}^{ht}.

Although the behavior of the identified parameters with frequency is not constant in Fig. 5a and b, it is known from the effect analysis performed [27] for the same assembly that the contact dynamics at the holder–tool interface controls mainly the tool mode of the tool point FRF. Hence, rather than considering the whole frequency band in the noisy plots of Fig. 5a and b, one should focus on the vicinity of the tool mode frequency and identify the interface parameters of the holder–tool interface from that region. Consequently, the translational stiffness and damping parameters identified in Fig. 5a and b at the frequency of the second vibration mode are in perfect agreement with those identified in Fig. 3a and b.

So far, the implementation of the identification approach proposed in this paper is demonstrated analytically with an example for extracting the holder–tool interface parameters for a typical spindle–holder–tool assembly. First, direct analytical FRFs are used as inputs and then they are distorted to simulate a more realistic scenario. It is observed that the results are in agreement with the effect analysis performed and the identification approach suggested in a recent work [27]. An experimental application of the identification approach is given in the following section.

4. Experimental verification for identification of contact dynamics at the holder–tool interface

In this section in addition to the analytical case study, an experimental case study for the identification approach described is provided. Experiments were performed with BT 40 type holder, in which a carbide tool of 16 mm diameter and 123 mm length is inserted with an overhang length of 49 mm, and is assembled to the free spindle. Spindle-holder–tool assembly is shown in Fig. 6. Experiments were performed with a laser vibrometer. By using the laser measurement technique, the mass loading effect of the accelerometers is avoided and accuracy of the method is improved since the method is highly sensitive to the measurement errors and noise in the measured data.

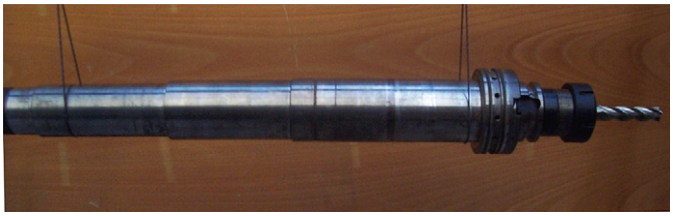

Fig. 6. Spindle–holder–tool suspended assembly for free–free measurements.

The tip-point receptance of the spindle–holder subassembly (without the tool part outside the holder) is obtained (by performing an impact test) as shown in Fig. 7a, and this is the first element of the assembly matrix [SH_{11}]. The tool point FRF of the assembly is obtained by performing impact test as shown in Fig. 7b, and this is the first element of the assembly matrix [SHT_{11}] as mentioned previously. As observed in Section 3, the noise in the measured data highly affects the identification method. Therefore, the experimentally obtained FRFs are filtered with the Savitzky–

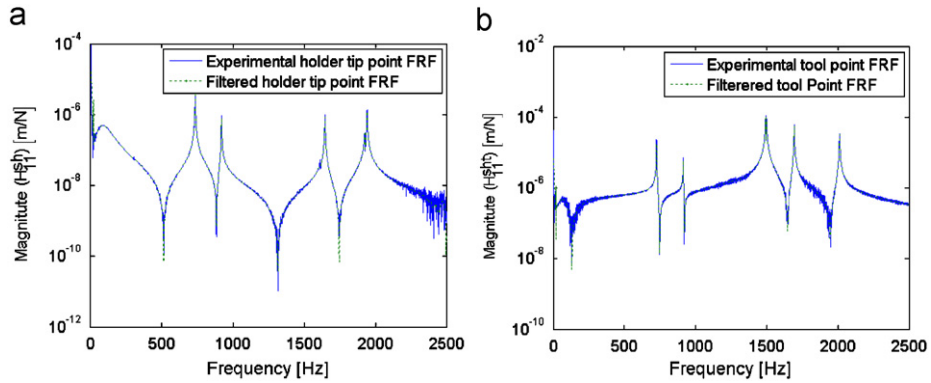

Fig. 7. (a) Experimentally obtained tip-point FRF (H_{11}^{sh}) of the spindle–holder subassembly and filtered tip-point FRF of the spindle holder subassembly and (b) experimentally obtained tool point FRF (H_{11}^{sht}) of the spindle–holder–tool assembly and filtered tip-point FRF of the spindle–holder–tool assembly.

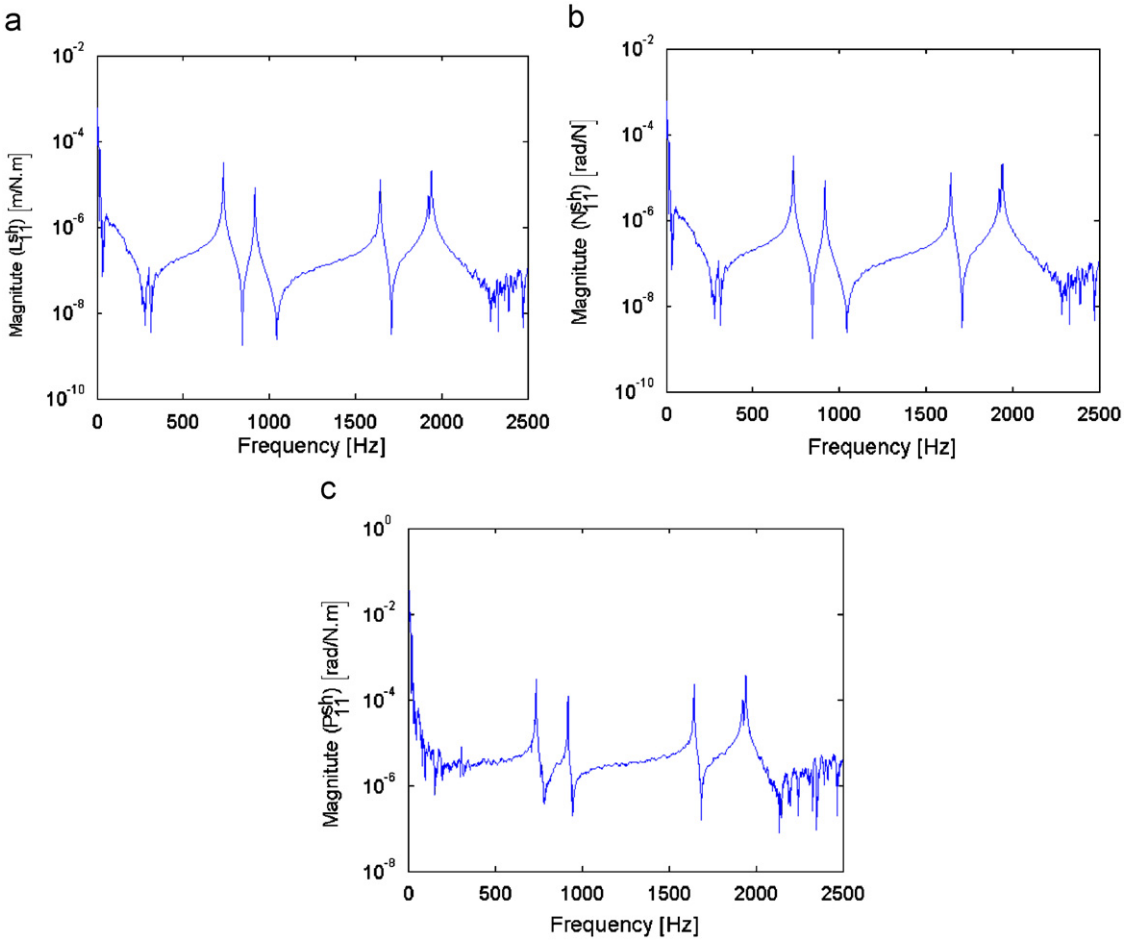

Fig. 8. (a) Approximately obtained tip-point FRF (L_{11}^{sh}) of the spindle–holder subassembly, (b) approximately obtained tip-point FRF (N_{11}^{sh}) of the spindle–holder subassembly and (c) approximately obtained tip-point FRF (P_{11}^{sh}) of the spindle–holder subassembly.

Golay filter [31]. The filtered tip-point FRF of the spindle–holder subassembly and filtered tool point FRF of the spindle–holder–tool assembly are given in Fig. 7a and b, respectively, along with the original FRFs.

In order to obtain angular displacement or moment-related FRFs of $[SH_{11}]$ and $[SHT_{11}]$, second-order approximation is used given by Duarte and Ewins [30] with spacing 35 and 40 mm between measurement points for the holder–spindle subassembly and spindle–holder–tool assembly, respectively. The resulting FRFs of the $[SH_{11}]$ and $[SHT_{11}]$ matrices are shown in Figs. 8 and 9, respectively. It is important to note that the accuracy of the method depends on the spacing between measurement points and the order of the approximation method [30]. As expressed by Duarte and Ewins [30], increasing the approximation order requires smaller spacing (between the measurement points) for the angular displacement-to-force FRFs, whereas it requires larger spacing for the angular displacement-to-moment FRFs. Although the effect of spacing between the measurement points was not

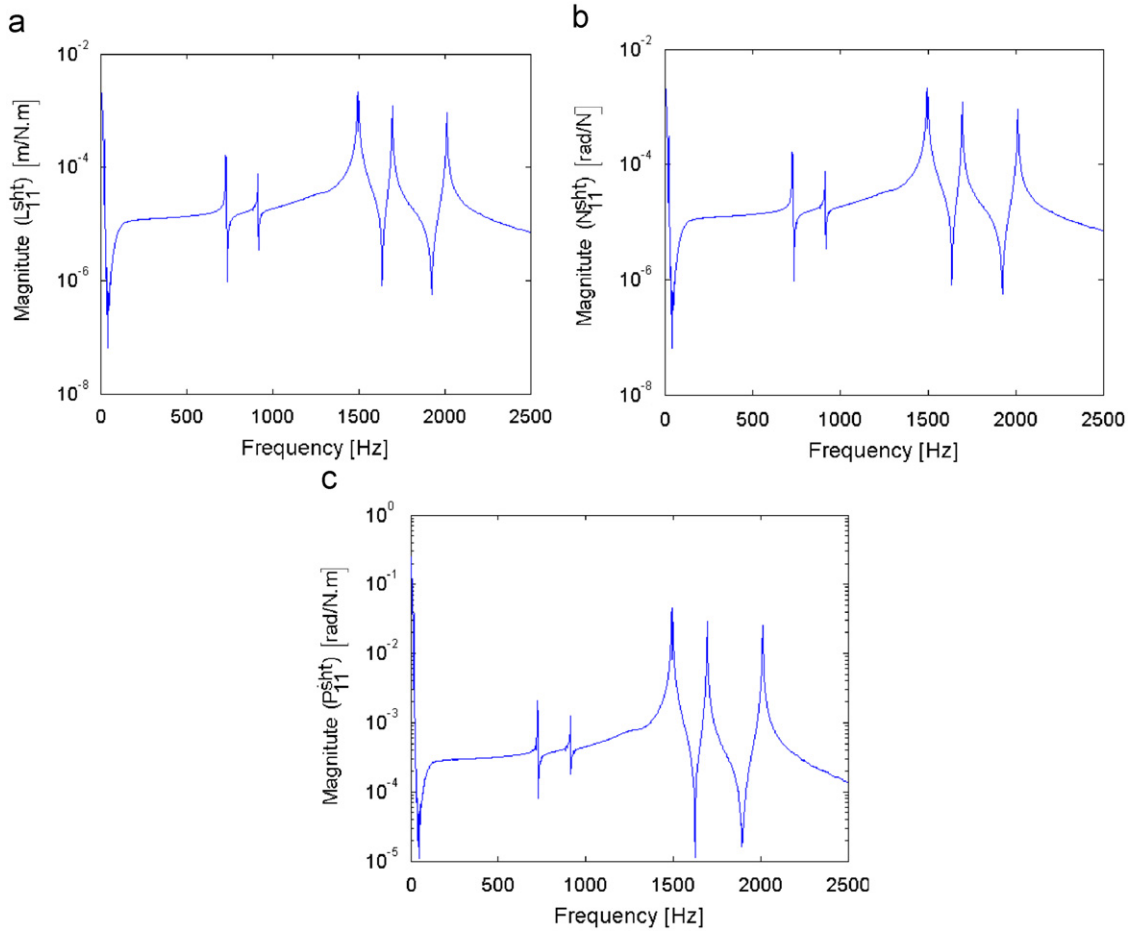

Fig. 9. (a) Approximately obtained tool point FRF (L_{11}^{sht}) of the spindle–holder–tool assembly, (b) approximately obtained tool point FRF (N_{11}^{sht}) of the spindle–holder–tool assembly and (c) approximately obtained tool point FRF (P_{11}^{sht}) of the spindle–holder–tool assembly.

tested systematically, it has been observed in this work that the measurement spacing had an impact on the identified parameters. Here, a practical value of 35 mm for the spindle–holder sub-assembly and 40 mm for the spindle–holder–tool assembly are taken for the measurement spacing values, which compromises measurement time and accuracy is selected based on initial measurements. Optimizing the measurement spacing for an acceptable accuracy and time may be an interesting subject for future research. As an alternative, one can use rotary sensors to eliminate this problem at the expense of increased sensor cost.

The receptance matrices of the cutting tool in free–free boundary conditions, which are denoted by $[T_{11}]$, $[T_{12}]$, $[T_{21}]$ and $[T_{22}]$, are obtained analytically. After obtaining the FRFs required for constructing the right-hand side of Eq. (6), the complex stiffness matrix $[K_{ht}]$ is obtained from Eq. (6). Then, the linear displacement-to-force, linear displacement-to-moment, angular displacement-to-force and angular displacement-to-moment complex stiffness functions of the holder–tool interface are obtained (which are, respectively, $k_{yf}^{ht}+i\omega c_{yf}^{ht}$, $k_{ym}^{ht}+i\omega c_{ym}^{ht}$, $k_{\theta f}^{ht}+i\omega c_{\theta f}^{ht}$ and $k_{\theta m}^{ht}+i\omega c_{\theta m}^{ht}$).

It is known from the typical spindle–holder–tool assembly investigated by Ertürk et al. [27] that the holder–tool connection parameters mainly affect the tool-dominant vibration mode. Hence, it is reasonable to identify the holder–tool contact parameters from this mode. As seen from Fig. 7b, the tool point FRF of the assembly shown in Fig. 6 has four distinct modes in the frequency range of interest. Therefore, in order to identify the tool-dominant mode, the assembly tool point FRF is measured for

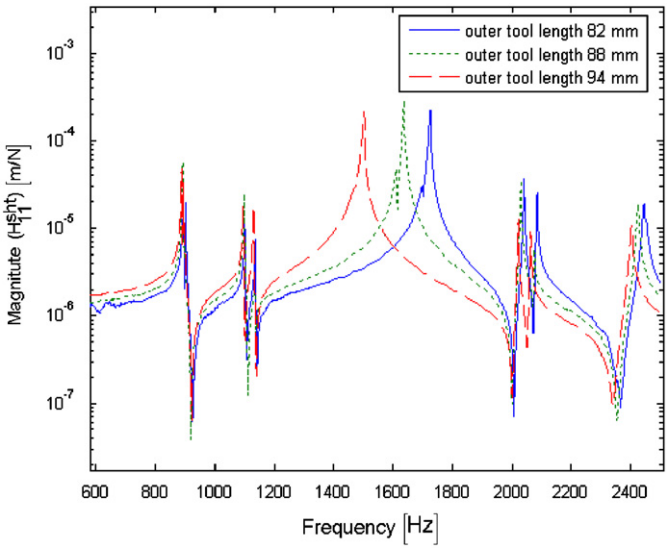

Fig. 10. Tool point FRF with changing tool length outside the holder.

different overhang lengths of the tool. The three different overhang lengths taken are 82, 88 and 94 mm. For these three configurations, it is observed that the third mode is mainly

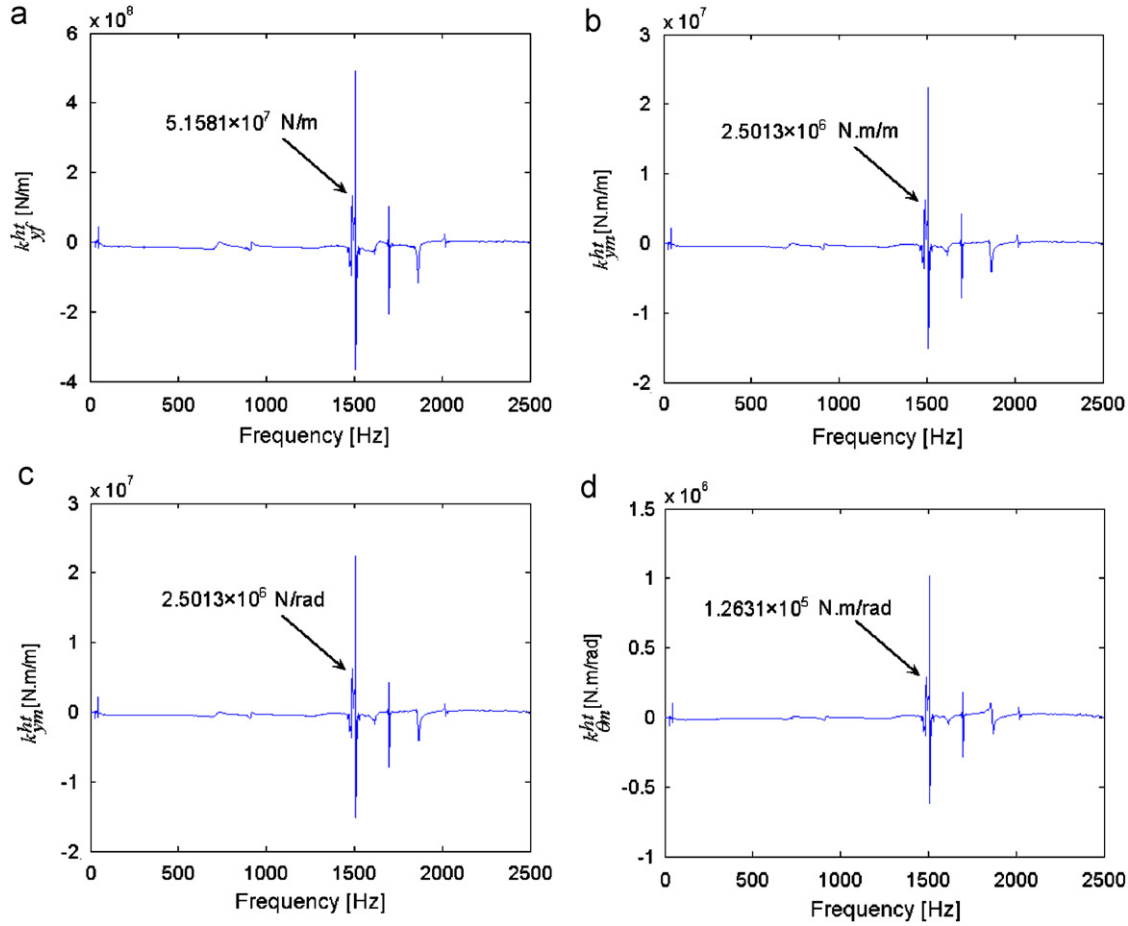

Fig. 11. Identified stiffness values at the holder–tool interface obtained from Eq. (6) by using the filtered experimental FRFs (a) linear displacement-to-force stiffness, (b) linear displacement-to-moment stiffness, (c) angular displacement-to-force stiffness and (d) angular displacement-to-moment stiffness.

affected by the tool overhang length as shown in Fig. 10. Therefore, the third vibration mode in the tool point FRF is the tool mode and the holder–tool contact dynamics can be identified from this mode.

For a tool overhang length of 49 mm, the identified linear/angular displacement-to-force/moment stiffness FRFs are shown in Fig. 11a–d, whereas the identified damping FRFs are given in Fig. 12a–d. Detailed view of the identified linear displacement-to-force stiffness values with the tool point FRF is also given in Fig. 13. Note that, since the holder–tool connection parameters are to be identified at the frequency of the tool-dominant mode (see Fig. 10), one can read the contact parameters of the holder–tool interface as presented in Table 2. Note that the *L* and *N* FRFs are taken to be identical in Figs. 8 and 9 for convenience (with the assumption of reciprocity), and six distinct values have been identified.

In order to show the accuracy of the identification method, the experimentally obtained spindle–holder subassembly receptance matrix $[SH_{11}]$ is coupled with analytically obtained tool FRFs through the *forward* coupling equation, Eq. (5). In coupling of the spindle–holder and tool subsystems, instead of using frequency-dependent contact parameters (depicted in Figs. 11 and 12), the constant values identified from the respective dominant mode of the holder–tool interface (Table 2) are used. Fig. 14 shows the experimentally obtained tool point FRF along with the one obtained from the receptance coupling equation (Eq. (5)) where the holder–tool interface stiffness matrix is constructed with the parameters identified in Table 2. It can be seen from Fig. 13 that the identification method presented in this paper works very successfully.

5. Conclusions

Recent literature on modeling and analysis of spindle–tool assemblies has shown the importance of contact dynamics for accurate prediction of chatter stability. In particular, the contact dynamics at the spindle–holder and holder–tool interfaces have a strong impact on the tool point frequency response. The stiffness and damping parameters of these critical interfaces affect the prediction of chatter frequencies and depth of cut limits, respectively. In this paper, a new approach is presented for identification of dynamical contact parameters in spindle–holder–tool assemblies. The elastic receptance coupling equations previously used for coupling the system components (spindle, holder and tool) are rearranged to give the complex stiffness matrix at the holder–tool and spindle–holder interfaces in a closed-form manner. First, an analytical demonstration of the identification approach is presented for a given assembly. Then, the analytical data are distorted with random noise and the coherence between the analytical FRFs is reduced. It is observed that the method is highly sensitive to noise in the FRF data, although it is still possible to identify the correct dynamical contact parameters from the relevant vibration modes. This sensitivity is expected to be mainly due to matrix inversions involved in the method. This experience

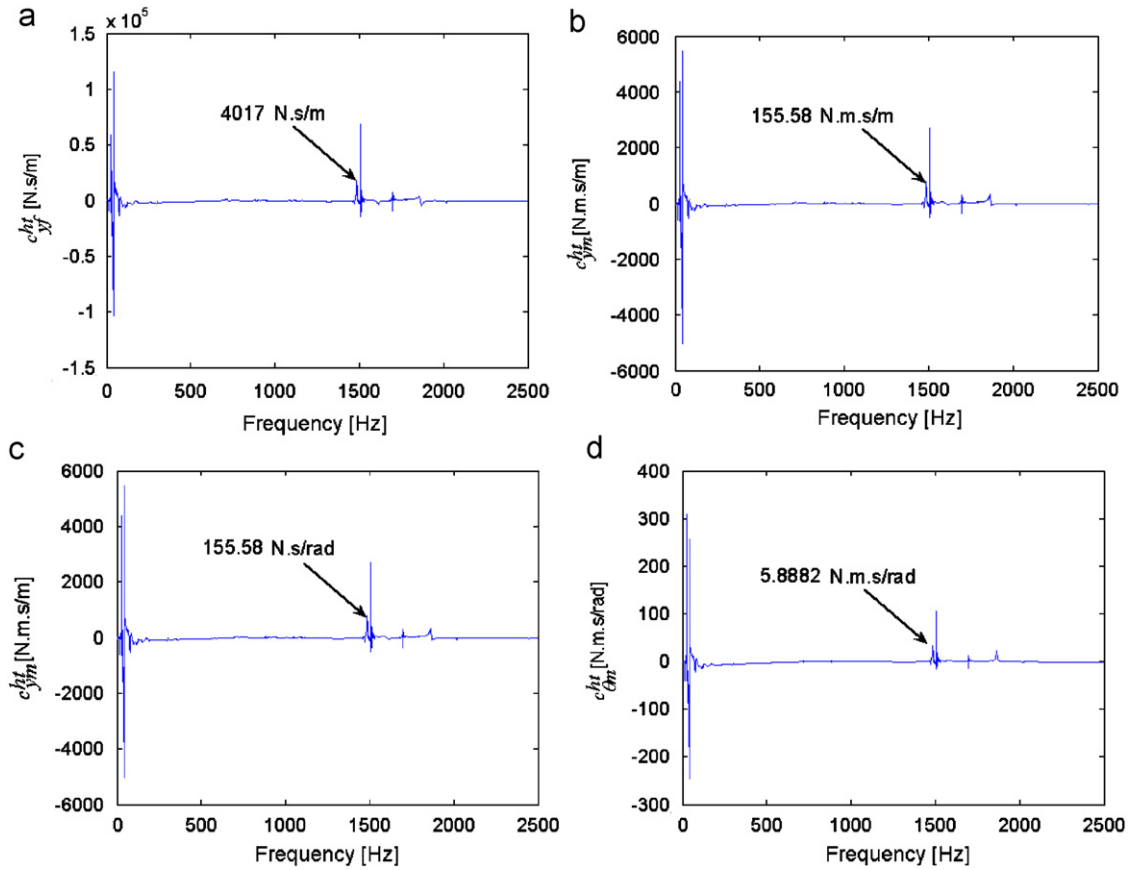

Fig. 12. Identified stiffness values at the holder–tool interface obtained from Eq. (6) by using the filtered experimental FRFs (a) linear displacement-to-force damping, (b) linear displacement-to-moment damping, (c) angular displacement-to-force damping and (d) angular displacement-to-moment damping.

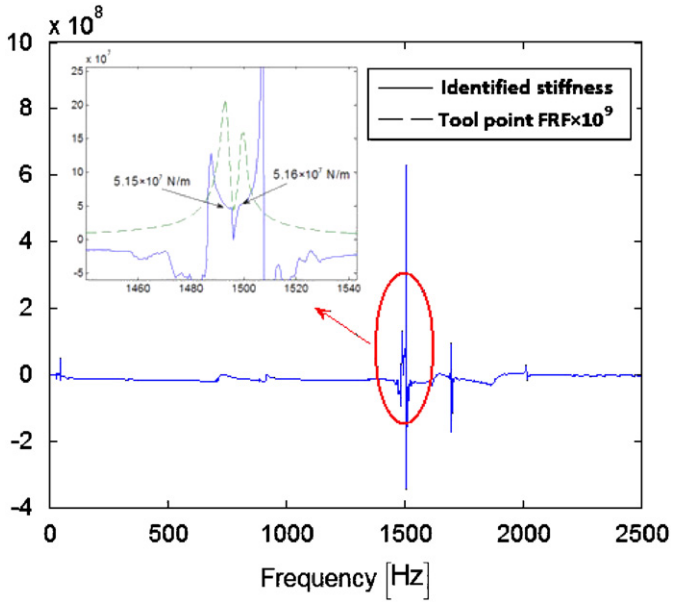

Fig. 13. Identified linear displacement-to-force stiffness values at the holder–tool interface obtained from Eq. (6) by using the filtered experimental FRFs.

highlights the importance of filtering the noise in the experimental FRFs before using them in the identification.

The identification approach proposed in this paper is also experimentally verified by using it in a spindle–holder–tool assembly (with a focus on the holder–tool interface). Due to the aforementioned sensitivity of the formulation, the measured FRFs are minimized by employing the Savitzky–Golay filter. The accuracy of the identification approach also depends on the accuracy of the experimentally obtained rotation and moment-related FRFs. The rotation and moment-related FRFs are approximated by using the measured translational FRFs in an existing method from the literature of experimental modal analysis. In the experimental verification, attention is given to the holder–tool interface of the assembly and it is shown that the contact parameters of this interface can be identified successfully from the relevant vibration mode it controls. Although the identification approach presented in this paper considered the contact dynamics at the spindle–holder and holder–tool interfaces of the assembly, the method can be extended to identify bearing dynamics and the dynamics of the other critical joints in a similar manner.

Table 2
Identified dynamical contact parameters at the holder–tool interface in the experimental case study

Linear displacement-to-force stiffness (N/m)	5.1581×10^7
Linear displacement-to-force damping (N s/m)	4017
Linear displacement-to-moment stiffness (N m/m)	2.5013×10^6
Linear displacement-to-moment damping (N m s/m)	155.58
Angular displacement-to-force stiffness (N/rad)	2.5013×10^6
Angular displacement-to-force damping (N s/rad)	155.58
Angular displacement-to-moment stiffness (N m/rad)	1.2631×10^5
Angular displacement-to-moment damping (N m s/rad)	5.8882

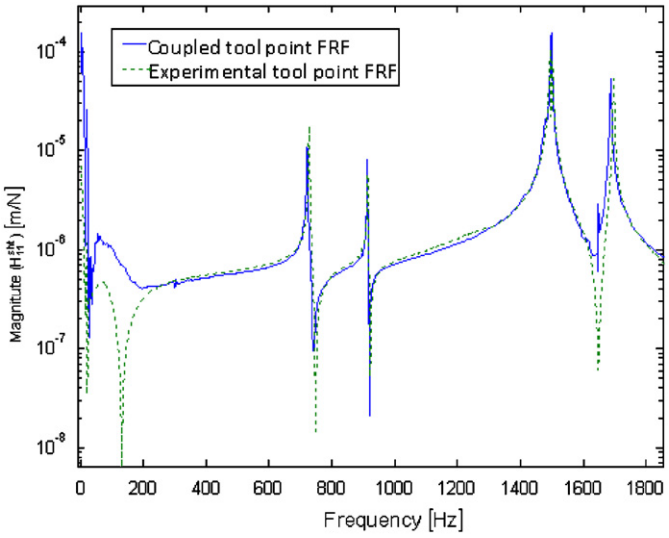

Fig. 14. Experimentally obtained tool point FRF and the tool point FRF obtained by receptance coupling with the identified contact parameters.

Acknowledgement

This project is funded by the Scientific and Technological Research Council of Turkey (TUBITAK) under Project number 104M430 which is gratefully acknowledged.

References

[1] S.A. Tobias, W. Fishwick, The chatter of lathe tools under orthogonal cutting conditions, Transactions of ASME 80 (1958) 1079–1088.
[2] J. Tlusty, M. Polacek, The stability of machine tools against self-excited vibrations in machining, in: Proceedings of the ASME International Research in Production Engineering, Pittsburgh, USA, 1963, pp. 465–474.
[3] I. Minis, T. Yanushevsky, R. Tembo, R. Hocken, Analysis of linear and nonlinear chatter in milling, Annals of the CIRP 39 (1990) 459–462.
[4] Y. Altintas, E. Budak, Analytical prediction of stability lobes in milling, Annals of the CIRP 44 (1995) 357–362.
[5] E. Budak, Y. Altintas, Analytical prediction of chatter stability in milling—part I: general formulation; part II: application to common milling systems, Transactions of ASME, Journal of Dynamic Systems, Measurement, and Control 120 (1998) 22–36.
[6] Y. Altintas, Manufacturing Automation, Cambridge University Press, New York, NY, 2000.
[7] T. Schmitz, R. Donaldson, Predicting high-speed machining dynamics by substructure analysis, Annals of the CIRP 49 (1) (2000) 303–308.
[8] T. Schmitz, M. Davies, M. Kennedy, Tool point frequency response prediction for high-speed machining by RCSA, Journal of Manufacturing Science and Engineering 123 (2001) 700–707.
[9] T. Schmitz, M. Davies, K. Medicus, J. Snyder, Improving high-speed machining material removal rates by rapid dynamic analysis, Annals of the CIRP 50 (1) (2001) 263–268.
[10] R.E.D. Bishop, D.C. Johnson, The Mechanics of Vibration, Cambridge University Press, Cambridge, 1960.
[11] J.V. Ferreira, D.J. Ewins, Nonlinear receptance coupling approach based on describing functions, in: Proceedings of the 14th International Modal Analysis Conference, Dearborn, MI, 1996, pp. 1034–1040.
[12] W. Liu, D.J. Ewins, Substructure synthesis via elastic media, Journal of Sound and Vibration 257 (2) (2002) 361–379.
[13] S.S. Park, Y. Altintas, M. Movahhedy, Receptance coupling for end mills, International Journal of Machine Tools and Manufacture 43 (2003) 889–896.
[14] E.B. Kivanc, E. Budak, Structural modeling of end mills for form error and stability analysis, International Journal of Machine Tools and Manufacture 44 (2004) 1151–1161.
[15] G.S. Duncan, T. Schmitz, An improved RCSA model for tool point frequency response prediction, in: Proceedings of the 23rd International Modal Analysis Conference, January 30–February 3, 2005, Orlando, FL (on CD).
[16] K.L. Johnson, Contact Mechanics, Cambridge University Press, Cambridge, 1985.
[17] E.I. Rivin, Stiffness and Damping in Mechanical Design, Marcel Dekker, Inc., New York, 1999.
[18] E.I. Rivin, Influence of tool holder interfaces on tooling performance, Transactions of NAMRI/SME (1993) 173–179.
[19] M. Weck, I. Schubert, New interface machine/tool: hollow shank, Annals of the CIRP 43 (1) (1994) 345–348.
[20] J. Agapiou, E. Rivin, C. Xie, Tool holder/spindle interfaces for CNC machine tools, Annals of the CIRP 44 (1) (1995) 383–387.
[21] S. Smith, T.P. Jacobs, J. Halley, The effect of drawbar force on metal removal rate in milling, Annals of the CIRP 48 (1) (1999) 293–296.
[22] T. Schmitz, K. Powell, D. Won, G.S. Duncan, W.G. Sawyer, J.C. Ziegert, Shrink fit tool holder connection stiffness/damping modeling for frequency response prediction in milling, International Journal of Machine Tools and Manufacture 47 (2007) 1368–1380.
[23] K. Ahmadi, H. Ahmadian, Modeling machine tool dynamics using a distributed parameter tool–holder joint interface, International Journal of Machine Tools and Manufacture 47 (2007) 1916–1928.
[24] A. Ertürk, H.N. Özgüven, E. Budak, Analytical modeling of spindle–tool dynamics on machine tools using Timoshenko beam model and receptance coupling for the prediction of tool point FRF, International Journal of Machine Tools and Manufacture 46 (2006) 1901–1912.
[25] E. Budak, A. Ertürk, H.N. Özgüven, A modeling approach for analysis and improvement of spindle–holder–tool assembly dynamics, Annals of the CIRP 55 (2006) 369–372.
[26] A. Ertürk, E. Budak, H.N. Özgüven, Selection of design and operational parameters in spindle–holder–tool assemblies for maximum chatter stability by using a new analytical model, International Journal of Machine Tools and Manufacture 47 (2007) 1401–1409.
[27] A. Ertürk, H.N. Özgüven, E. Budak, Effect analysis of bearing and interface dynamics on tool point FRF for chatter stability in machine tools by using a new analytical model for spindle–tool assemblies, International Journal of Machine Tools and Manufacture 47 (2007) 23–32.
[28] A. Ertürk, Dynamic modeling of spindle–tool assemblies in machining centers, M.S. Thesis, Department of Mechanical Engineering, Middle East Technical University, Ankara, Turkey, May 2006.
[29] I.S. Sokolnikoff, Mathematical Theory of Elasticity, McGraw-Hill, New York, 1946.
[30] M.L.M. Duarte, D.J. Ewins, Rotational degrees of freedom for structural coupling analysis via finite-difference technique with residual compensation, Mechanical Systems and Signal Processing 14 (2) (2000) 205–227.
[31] A. Savitzky, M.J.E. Golar, Smoothing and differentiation of data by simplified least squares procedures, Analytical Chemistry 36 (1964) 1627–1639.